[AMERICAN JOURNAL OF SCIENCE, VOL. 287, JANUARY, 1987, P. 50-76]

THE COMPOSITION OF CHLORITE AS A FUNCTION OF SULFUR AND OXYGEN FUGACITY: AN EXPERIMENTAL STUDY

L. TARAS BRYNDZIA* and STEVEN D. SCOTT
Department of Geology, University of Toronto,
170 College Street, Toronto, Ontario Canada M5S 1A1

ABSTRACT. Observations in nature of systematic variations in the iron content of chlorite, in rocks of variable bulk composition and metamorphic grade, have been successfully modelled experimentally in terms of the relative stability of iron–magnesium chlorite as a function of fO_2, fS_2, P, and T. The two reactions for which equilibrium fO_2–fS_2–chlorite compositions have been determined are:

$$\text{Sulfidation: } Fe_5Al_2Si_3O_{10}(OH)_8 \text{ (in Fe–Mg chlorite)} + 5/2S_2 = Al_2SiO_5 + FeS \text{ (in pyrrhotite)} + 2SiO_2 + 5/2O_2 + 4H_2O \quad (1)$$

$$\text{Oxidation: } Fe_5Al_2Si_3O_{10}(OH)_8 \text{ (in Fe–Mg chlorite)} + 5/6O_2 = Al_2SiO_5 + 5/3Fe_3O_4 + 2SiO_2 + 4H_2O \quad (2)$$

Chlorites of variable composition, equilibrated reversibly at oxygen and sulfur fugacities buffered by the pyrite–pyrrhotite–magnetite (PPM) assemblage or those defined by coexisting pyrrhotite and magnetite, produced consistent Fe/(Fe + Mg) ratios in chlorite run products at a given pressure and temperature. Equilibrium Fe/(Fe + Mg) ratios in chlorite are a function of the ambient oxygen and sulfur fugacity conditions and are independent of bulk charge compositions. Bulk charge compositions do dictate stable mineral assemblages, however.

A one-site chlorite solution model given by the expression: $a_{Daph} = [Fe^{2+}/\Sigma X(Oct) = 6.00/5/6]\,[Al(Oct)/\Sigma X(Oct) = 6.00)/1/6]^{1/5}$, in which iron and aluminum mix randomly over available octahedral sites, and mixing of silicon and aluminum in tetrahedral sites may be ignored, has been derived from model activity-composition relationships determined from electron microprobe analyses of chlorite run products. Activities of daphnite calculated from the model are equivalent, within analytical error, to the mole fraction of iron in the chlorite formula, indicating that solution of the daphnite component in chlorite may be taken to be ideal for the range of chlorite compositions encompassed by the experiments ($Fe/\Sigma R^{2+} = 0$ to 0.4).

The standard state enthalpy and free energy of formation of the stoichiometric iron-endmember chlorite, from the elements at 298.15K and 1 bar have been extrapolated from logK versus 1/T(K) and ΔG_r° versus T(K) plots over the 50°C interval of the experiments. These are: $\Delta H_f^\circ = -1726.35 \pm 11$ kcal/mole and $\Delta G_f^\circ = -1600.7 \pm 6.4$ kcal/mole respectively. The absolute standard state entropy of formation (S_f°) at 298.15K and 1 bar is calculated to be 142.2 ± 13 cal/mol/K.

* Present address: The James Franck Institute, The University of Chicago, 5640 Ellis Avenue, Chicago, Illinois 60637

The experimental chlorite data may be applied directly to rocks containing the assemblage chlorite + quartz + Al_2SiO_5 +/− oxides +/− sulfides. Application of our results to the metamorphosed amphibolite grade sulfide ores and country rocks of Ducktown, Tenn. show that agreement between the predicted and observed composition of chlorite coexisting with quartz + kyanite, at the transition of ilmenite to rutile + pyrrhotite, is excellent.

INTRODUCTION

Chlorite is an ubiquitous and commonly abundant mineral in a wide variety of geological settings, particularly in low to moderate grade metamorphic rocks and in zones of hydrothermal alteration associated with several different types of ore deposits. Petrogenetic studies involving assemblages of ferromagnesian silicates coexisting with opaque phases such as pyrite, pyrrhotite, magnetite, hematite, and Fe–Ti oxides, have revealed variations in the Fe/(Fe + Mg) ratio of those silicates, depending on the associated opaque phases (Chinner, 1960; Mueller, 1960; Kanehira, Banno, and Nishida, 1964; Hounslow and Moore, 1967; Annersten, 1968; Kramm, 1973; Rumble, 1974; Guidotti, 1974; and Nesbitt and Kelly, 1980). The variations in silicate mineral composition were attributed by Hounslow and Moore (1967), Kramm (1973), and Rumble (1974) to the fugacity of oxygen (fO_2), as predicted by Chinner (1960). Of particular relevance to the present study, Rumble (1976) demonstrated that an increase in the $Fe_2O_3/(Fe_2O_3 + TiO_2)$ ratio in ilmenite, controlled by increasing fO_2, correlated with a decrease in the Fe/(Fe + Mg) ratio of coexisting chlorite.

Other studies, on regionally metamorphosed sulfidic pelites, attributed the systematic changes in mineral composition to reactions between the ferromagnesian silicates and sulfur (for example, Marmo, 1957, 1960; Peltola, 1960; Mallio and Gheith, 1972; Thompson, 1972; Guidotti, 1974; Mohr and Newton, 1983). Observed trends of decreasing Fe/(Fe + Mg) ratio in ferromagnesian silicates with proximity to an ore body, particularly in regionally metamorphosed terrains, have been attributed to sulfide–oxide–silicate equilibria established during metamorphism (McDonald, 1967; Froese, 1971, 1976, 1977; Craig and Gilbert, 1974; Koo and Mossman, 1975; Popp, 1976; Popp, Gilbert, and Craig, 1977; Hutcheon, 1979; Tso, Gilbert, and Craig, 1979; and Nesbitt and Kelly, 1980). In particular, such compositional trends for chlorite have been documented in rocks ranging from greenschist to amphibolite grade (Nash, 1973; Large, 1975; Bachinski, 1976; Kalogeropoulos, ms; and Nesbitt, 1982). Therefore, the trends observed in compositions of ferromagnesian silicates from an assemblage of sulfide–oxide–silicate minerals can be explained by oxidation and/or sulfidation processes, a point originally made by Kullerud and Yoder (1963, 1964).

Problems arise, however, in attempts to calculate the stability of chlorite in large part due to a lack of thermodynamic data for daphnite, the Fe-endmember. Since chlorite is such a common mineral, it is desirable to calibrate experimentally the dependence of chlorite composition

from a specified assemblage as a function of fO_2 and fS_2. Phase relations outside the experimental range can be calculated from the derived thermodynamic data by assuming a solution model. Observations in nature can then be interpreted in light of such phase relations. The aim of our hydrothermal experiments was to determine values of fO_2 and fS_2 for the oxidation and sulfidation of chlorite of different compositions in the presence of quartz and aluminosilicate, under conditions of $P_{Total} = P_{H_2O}$ over a temperature and pressure interval of 575° to 625°C and 2.07 to 6.0 kb. Our results are directly applicable to medium and high grade metamorphic terrains which contain the requisite mineral assemblage and for which chlorite does not contain appreciable ferric iron.

PREVIOUS STUDIES

Kullerud and Yoder (1963, 1964) showed by preliminary sulfidation experiments involving ferromagnesian silicates that sulfur combines with some of the silicate Fe^{2+} to form sulfides and some of the Fe^{2+} reacts with oxygen made available by the decomposition of the silicate to form oxides. The assemblage produced by the sulfidation reaction consists of a ferromagnesian silicate lower in Fe/(Fe + Mg) coexisting with an iron sulfide and an iron oxide determined by the fS_2 and fO_2 of the experiment. Kullerud and Yoder also pointed out that even a few percent sulfur was capable of changing the oxidation state of a rock without the addition or subtraction of oxygen. Other experimental studies followed including equilibrium compositions of coexisting Fe–Ni monosulfide solid solution and olivine (Clark and Naldrett, 1972), Co–Ni partitioning between orthopyroxene and sulfides (Rajamani, 1976), and compositions of coexisting pyrrhotite and pyroxene (Naldrett and Brown, 1968), biotite (Hammarback and Lindqvist, 1972), and amphibole (Popp and Gilbert, 1974).

Hydrothermal experiments on biotites were performed by Hammarback and Lindqvist (1972) by using an oxide mix plus sulfur in Au tubes. Although their results showed a general trend of more sulfur-rich pyrrhotite coexisting with more Mg-rich biotites, they did not demonstrate equilibrium. An improvement was made in experiments with coexisting pyrrhotite and orthoamphibole by Popp, Gilbert, and Craig (1977), who modified previous hydrothermal techniques in order to assure reversibility. This method was later adopted by Tso, Gilbert, and Craig (1979) who equilibrated pyrrhotite–biotite along the join annite–phlogopite. We have further modified these procedures in our work.

EXPERIMENTAL AND ANALYTICAL METHODS

Hydrothermal Techniques

The hydrothermal techniques used in our oxidation-sulfidation experiments are similar to those employed in previous studies in this laboratory and have been discussed in detail by McOnie, Fawcett, and James (1975), Fleming and Fawcett (1976), and Allen and Fawcett (1982).

Experiments conducted at 2.07 kb used water as the pressure medium and were run in vertically mounted Tuttle (1949) cold-seal vessels made

of Rene 41 alloy. Pressure was measured on a 50,000 psi Heise gauge to an accuracy of ± 50 bars. The temperatures of the experiments were read from internally fitted thermocouples (in contact with the capsules) and measured with a calibrated Thermo Electric Minimite potentiometer. Total estimated uncertainty in measured run temperatures is ± 7°C.

Experiments at higher pressures (4.5-6.0 kb) were conducted in vertically mounted Luth and Tuttle (1963) cold-seal Rene 41 alloy vessels with a modified closure assembly (Fawcett, Davies, and James, 1971) and with argon gas as the pressure medium. Bird (ms) has described in detail the operation of this equipment. Pressures were monitored by manganin cells connected to Foxboro chart recorders calibrated against a Heise gauge and are accurate to ± 50 bars. Temperatures were monitored as for the lower pressure experiments with a total estimated uncertainty of ± 8°C.

Starting Materials

Chlorite.—Samples of natural chlorite were obtained from the mineralogy collections at the Royal Ontario Museum and the American Museum of Natural History and were selected solely on the basis of optical purity, 14Å structure, compositional homogeneity based on electron microprobe analysis, and balanced structural formulae. All starting chlorite compositions are listed in the first six columns of table 2. Chlorites 1, 3, and 10 are ROM samples M6380, M6372, and M36846, and chlorites 4, 16, and 17 are AMNH samples 13669, 13706, and 13733, respectively. The chlorite was separated into pieces (where possible) with the aid of a binocular microscope, ground in an agate mortar and sieved to −100 mesh size.

Quartz.—Brazilian optical grade quartz from the mineralogy collection of the Department of Geology at the University of Toronto was the source of SiO_2. It was crushed by hand in an agate mortar and sieved to −160 mesh size, washed in a boiling concentrated solution of HCl and distilled water, rinsed several times with distilled water, oven dried at 110°C overnight, and then stored in a dessicator.

Al_2SiO_5.—All three aluminosilicate polymorphs were utilized, as dictated by the pressure and temperature conditions of a given experiment. Gem quality kyanite from Georgia, USA was obtained from the mineralogy collection of the Department of Geology at the University of Toronto. Large (2 cm long) optically homogeneous blades of this mineral were crushed by hand in an agate mortar and sieved to −160 mesh size, treated, and stored in the same manner as for quartz. Pink gem quality andalusite from the Minas Gerais district of Brazil was obtained from the collections of the Mineralogy Department at the Royal Ontario Museum (ROM sample M24093). Sample preparation was as described for kyanite. Sillimanite was purchased commercially as needles measuring up to 1 cm in length and up to 2 to 3 mm in diameter. Some grains were intergrown with quartz and very minor amounts of muscovite and biotite. Neither alteration of sillimanite nor the fibrolite polymorph were observed in thin section. Sillimanite was hand picked to a purity estimated to be at least

99 percent. Sample preparation was as described above for the kyanite, andalusite, and quartz.

Electron microprobe analysis indicated that the aluminosilicates are essentially pure phases, with only very minor concentrations of ferric iron, approx 0.3 wt percent Fe_2O_3 in andalusite and sillimanite, and 0.2 wt percent in kyanite. Mn, if present, must be in concentrations below the level of detection by energy dispersive microprobe analysis (approx 0.1 wt percent Mn).

Magnetite.—Magnetite was hydrothermally recrystallized from Fisher purified ferric-ferrous black oxide (lot #750848) in sealed gold capsules (with excess distilled water) at 750°C and 2.07 kb for 1 week. The Rene 41 alloy vessels are believed to have maintained the oxygen fugacity at conditions close to the nickel-nickel oxide fO_2 buffer.

Sulfides.—Pyrrhotite of troilite (FeS) composition was synthesized from stoichiometric proportions of Fe and S using the standard evacuated silica tube techniques described in detail by Kullerud (1971) and Scott (1974). Specpure sulfur crystals (JMC Ltd., lot #80371F) and Specpure Fe (JMC Ltd., lot #58261A) were the source of sulfur and iron, respectively. Iron was heated in a stream of hydrogen gas for 6 hrs at 750°C to remove any oxide coatings. Water and oxygen were removed from the hydrogen gas by first passing it over zinc metal at 395°C. Natural pyrite from Elba, Italy was the source of FeS_2. Spectrographic analysis reported in Scott (1973) gave as major impurities 1000 ppm Co, 100 ppm Cr, 100 ppm Pb, 50 ppm Ni, 10 ppm Mn, and 10 ppm Cu. All sulfides were crushed in an agate mortar and sieved to −100 mesh size.

The pyrite–pyrrhotite–magnetite (PPM) assemblage used in most of the experiments as an fO_2–fS_2 buffer was mixed in molar proportions of 3:3:2. The troilite–magnetite assemblage (PoMt buffer) was mixed in proportions of 3:1. All mixtures were stored in evacuated silica tubes to prevent oxidation.

Oxidation and Sulfidation of Chlorite

The experiments employed triple layer arrangements in double sealed gold capsules (fig. 1), modified from Popp, Gilbert, and Craig (1977). This configuration ensured that reversals could be obtained. The composition of the capsule material is an important consideration for experiments with sulfur. As was illustrated by Popp, Gilbert, and Craig (1977, fig. 4), several noble metals are not suitable capsule materials for assemblages containing pyrrhotite more sulfur-rich than N_{FeS} (mole fraction of FeS) of approx 0.970. Preliminary thermochemical calculations indicated that at the pressure and temperature conditions of the sulfidation-oxidation experiments in this study, pyrrhotite at the PPM triple point is considerably more sulfur-rich than $N_{FeS} = 0.970$, approx $N_{FeS} = 0.930$.

Because of the great difficulty in nucleating an aluminosilicate phase in early experiments, all charges in subsequent runs contained an aluminosilicate polymorph as part of the initial assemblage. Aluminosilicate and quartz were mixed in proportions of 2:3 together with equimolar

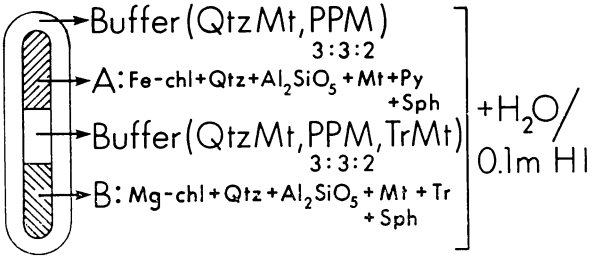

Fig. 1. Charge configuration used in sulfidation and oxidation experiments. See table 1 for abbreviation of phases.

proportions of chlorite, magnetite, and Fe–sulfide (that is, 1:1:1). Approx 5 volume percent sphalerite was included in most experiments in an attempt to monitor sulfur fugacity. However, sphalerite proved to be refractory, and these attempts were unsuccessful. All sulfur fugacities were calculated from pyrrhotite compositions obtained by electron microprobe analysis.

Capsules were prepared by first weighing approx 30 to 40 mg of the Mg–chlorite charge (B, see fig. 1) into the bottom of a gold capsule (3 mm OD) followed by the introduction of approx 30 mg of H_2O or 0.1 molal HI solution. Charges B and A (Fe–chlorite) were separated by a middle layer of material which consisted of 50 to 150 mg of either quartz + magnetite (3:2), PPM, or TrMt depending on the oxidation state required during the experiment (see table 1). The third layer consisted of 30 to 40 mg of the starting Fe–chlorite charge (A). The capsule was welded closed with a DC arc, ensuring minimal loss of volatiles. The inner capsules were sealed in an outer gold capsule (5.2 mm O.D) together with approx 150 to 200 mg of PPM buffer or quartz + magnetite and approx 70 mg of distilled water.

A 0.1 molal HI solution was used rather than distilled water as a flux in the later experiments in order to enhance recrystallization of the Fe–sulfides within the charges. Aqueous halide fluxes are used routinely in hydrothermal recrystallization experiments involving sulfides (Scott, 1974, 1975; Hutchison, ms). The HI flux should also promote recrystallization and equilibration of chlorite by enhancing the solution transport of cations such as Fe^{2+} between charges A and B in figure 1.

Electron Microprobe Analysis

All mineral compositions were determined by energy dispersive electron microprobe analysis using an Etec Autoprobe equipped with a Li-drifted Kevex Si detector and "on-line" data reduction using a "peak-stripping" programme (Statham, ms). Accelerating voltage was 20 kV with a beam current of 100 nA. Counting times were 200 sec for energy calibration on natural willemite (3000 cps) and intensity calibration on Co metal, and 100 sec (live-time) for all analyses.

Standards were as follows: Natural chlorite for Si, Al, Fe, Mn, and Mg in all chlorite analyses (Smith, 1969); synthetic pyrrhotite for Fe and S

TABLE 1

Summary of oxidation and sulfidation experiments using natural chlorite starting material. Numbers in parentheses refer to the following: (1) initial charge composition with chlorite from table 2 and the sulfide it was mixed with. (A) Fe–Chl + Qtz + Al_2SiO_5 + Mt + Py + Sp + 0.1 molal HI solution; (B) Mg–Chl + Qtz + Al_2SiO_5 + Mt + Tr + Sp + 0.1 molal HI solution. (2) Abbreviations for phases: An, andalusite; Chl, chlorite; Gh, ghanite/hercynite(ss); Ky, kyanite; Mt, magnetite; Mt(ss), magnetite/spinel(ss); Po, pyrrhotite; Py, pyrite; Qtz, quartz; Si, sillimanite; Sp, sphalerite; Tc, talc; Tr, troilite; Usp, ulvospinel/magnetite(ss). (3) Buffers: PPM, pyrite–pyrrhotite–magnetite; PoMt, pyrrhotite + magnetite

Run #	P (kb)	T (C)	Duration (days)	Charge (1) comp.		Products (2)	Buffer (3)
5	2.07	600	21	B	3+Tr	Chl-Tc-Mt(ss)-Po-Sp	PoMt
6	2.07	600	22	B	3+Tr	Chl-Tc-Mt(ss)-Po-Sp	PoMt
27	2.07	600	43	A	16+Py	Chl-Qtz-An-PPM-Sp	PPM
				B	17+Tr	Chl-Tc-Usp-An-PPM-Sp	PPM
28	2.07	600	43	A	17+Tr	Chl-Tc-Usp-An-PPM-Sp	PPM
26(b)	6.00	600	43	B	1+Tr	Chl-Qtz-Ky-PPM-Sp	PPM
30	6.00	600	43	A	16+Py	Chl-Qtz-Ky-PPM-Sp	PPM
				B	17+Tr	Chl-Tc-Qtz-Ky-Usp-PPM-Sp	PPM
31	6.00	600	43	A	1+Tr	Chl-Qtz-Ky-PPM	PPM
				B	17+Tr	Chl-Tc-Qtz-Ky-Usp-PPM	PPM
34	6.00	600	44	B	1+Tr	Chl-Qtz-Ky-Gh-PPM	PPM
36	6.00	600	55	A	10+Py	Chl-Qtz-Ky-Gh-Po-Mt	PoMt
				B	16+Py	Chl-Qtz-Ky-Gh-Po-Mt	PoMt
41	4.50	575	61	A	16+Py	Chl-Qtz-Si-PPM-Sp	PPM
				B	10+Py	Chl-Qtz-Si-PPM-Sp	PPM
42	5.00	600	61	B	1+Tr	Chl-Qtz-Si-PPM-Sp	PPM
43	5.50	625	61	B	1+Tr	Chl-Qtz-Si-PPM-Sp	PPM

in pyrrhotites. Pyrrhotite compositions are quoted as mole fraction FeS (N_{FeS}) in the FeS–S_2 system following Toulmin and Barton (1964).

Description of Phases in Run Products

The phase assemblages produced in the experiments are in table 1, electron microprobe analyses of product chlorite are in columns 7 to 23 of table 2, and analyses of pyrrhotite are in table 3.

Chlorite.—Chlorite ranged from 10 to 100 microns in size and, in general, was always in contact with all other phases (sulfide, oxide, and silicate). Most grains observed in polished thin section display yellow-green colors in plain light and low first order gray-yellow birefringence. Chlorite also occurs as fine-grained interstitial aggregates which host numerous inclusions of other phases. Both chlorite types were amenable to routine electron microprobe analysis and generally were of identical composition. However, occasional probe analyses of the fine-grained interstitial chlorite resulted in low oxide totals even though stoichiometry was maintained (see analyses of runs 41A and B in table 2). It is not known whether this is due to a problem of chlorite grain orientation or to dilution by adsorbed water during exposure to the beam.

Talc.—Talc occurs as wispy, distinctly micaceous grains, 10 to 100 microns in size and with high (third order) birefringence. It is commonly observed in relict patches of precursor chlorite which are recognized by a concentration of interstitial fine-grained (less than 5 microns) disseminated magnetite and pyrrhotite.

Al_2SiO_5.—Aluminosilicate was present in all run products of experiments 26 to 43, commonly occurring as well crystallized grains. In the high pressure runs (6.0 kb), laths of kyanite typically were corroded, strongly suggesting reaction of this phase. The exact nature of this reaction is not obvious and will be discussed in a later section.

Quartz.—Quartz was an ubiquitous phase in the products of all experiments with the exception of 5B, 6B, 27B, and 28A (2.07 kb runs) in which no quartz remained in Mg-rich charges. Quartz grains were generally between 20 to 100 microns in size and, rarely, were recrystallized into euhedra that displayed well developed crytal faces and/or terminations.

Spinel solid solutions.—Microprobe analyses of magnetite from runs 5B and 6B revealed overgrowths of a spinel which was indistinguishable from magnetite in reflected light. Identification of this phase was further complicated by the fact that it was never observed in the XRD traces which suggests that its concentration was very low, probably less than 10 volume percent. Microprobe analyses in subsequent runs indicated the presence of pure magnetite only.

Chlorite #17 (table 2) was the only Ti-bearing chlorite used, and, in run products of both 2.07 and 6.0 kb experiments, it was difficult to find chlorite sufficiently coarse to analyze, having in most cases been totally recrystallized to very fine-grained aggregates which host grains of ulvospinel–magnetite solid solution [Usp–Mt(ss)]. The Usp–Mt(ss) occurs as aggregates of well crystallized radiating laths commonly up to 100 microns in length which appear to have nucleated about very fine-grained magnetite apparently formed by oxidation of iron originally in the chlorite.

Some of the 6.0 kb runs lost sphalerite due to its consumption by a gahnite–hercynite forming reaction involving desulfidation of sphalerite and its reaction with kyanite, similar to experiments reported by Spry and Scott (1986).

TABLE 2

Summary of chlorite compositions used as starting materials in the sulfidation and oxidation experiments (columns 1-6) and compositions of chlorite run products (columns 7-23). All chlorite analyses are in wt percent, and formulae are reported as a unit half-cell based on 14 anhydrous oxygens, calculated as in Foster (1962). All iron is reported as ferrous iron, that is, FeO.

Run #							5B	6B	27A	27B	28A	26B	30A	30B	31A	31B	34B	36A	36B	41A	41B	42B	43B
T (C)							600	600	600	600	600	600	600	600	600	600	600	600	600	575	575	600	625
P (kb)							2.07	2.07	2.07	2.07	2.07	6.00	6.00	6.00	6.00	6.00	6.00	6.00	6.00	4.50	4.50	5.00	5.50
Buffer							PoMt	PoMt	PPM	PPM	PPM	PPM	PPM	PPM	PPM	PPM	PPM	PoMt	PoMt	PPM	PPM	PPM	PPM
	1	3	4	10	16	17																	
SiO_2	27.49	32.82	24.69	25.60	32.68	34.56	39.12	37.93	37.66	38.78	34.16	26.41	29.71	29.43	27.41	27.28	26.63	25.65	25.19	24.43	22.73	26.47	26.62
TiO_2	-	-	-	-	-	0.83	-	-	-	-	-	-	-	-	-	-	-	-	-	-	-	-	-
Al_2O_3	21.32	14.54	24.84	20.79	15.40	11.65	17.55	14.97	12.47	12.96	12.34	21.23	18.66	18.90	21.70	18.67	21.45	21.00	20.37	20.77	19.43	21.61	20.43
FeO*	12.58	4.28	16.07	22.77	26.27	6.15	12.78	12.97	8.60	7.99	7.31	12.73	14.24	14.91	13.23	14.53	13.56	21.30	20.97	18.28	15.61	12.38	11.04
MnO	0.04	-	0.12	-	0.40	0.12	0.15	0.11	0.19	0.06	0.10	-	0.39	0.36	-	0.18	-	-	-	-	-	-	-
MgO	26.16	34.36	21.84	18.12	13.62	31.39	20.73	19.86	26.23	28.71	30.06	24.98	23.56	23.12	25.88	23.33	24.02	18.04	17.84	17.57	17.43	24.79	25.53
CaO	-	-	-	-	0.88	-	-	-	-	-	-	-	-	-	-	-	-	-	-	-	-	-	-
Na_2O	0.29	0.48	0.15	0.29	-	0.51	-	-	-	-	-	-	-	-	-	-	-	-	-	-	-	-	-
K_2O	-	0.11	-	-	0.08	-	-	-	-	-	-	-	-	-	-	-	-	-	-	-	-	-	-
Total	87.87	86.59	87.72	87.57	89.33	85.20	90.33	85.84	85.16	88.50	83.97	85.35	86.56	86.72	88.21	84.01	85.65	86.07	84.39	81.24	75.20	85.26	83.39

Si	2.701	3.132	2.477	2.669	3.359	3.371	3.628	3.717	3.666	3.621	3.387	2.674	2.975	2.953	2.686	2.836	2.694	2.694	2.701	2.678	2.659	2.677	2.733
Ti (T)	-	-	-	-	-	0.061	-	-	-	-	-	-	-	-	-	-	-	-	-	-	-	-	-
Al (T)	1.299	0.868	1.523	1.331	0.641	0.578	0.372	0.283	0.344	0.380	0.613	1.326	1.026	1.047	1.314	1.164	1.306	1.306	1.299	1.322	1.341	1.323	1.267
Al (O)	1.169	0.768	1.415	1.224	1.225	0.802	1.546	1.446	1.097	1.047	0.839	1.208	1.188	1.188	1.193	1.123	1.253	1.294	1.275	1.362	1.340	1.252	1.205
Fe	1.034	0.342	1.348	1.985	2.259	0.502	0.991	1.063	0.700	0.624	0.606	1.078	1.193	1.252	1.085	1.263	1.150	1.879	1.881	1.677	1.527	1.047	0.948
Mn	0.004	-	0.010	-	0.034	0.010	0.012	0.009	0.016	0.004	0.008	-	0.034	0.030	-	0.016	-	-	-	-	-	-	-
Mg	3.832	4.886	3.267	2.816	2.087	4.566	2.865	2.902	3.806	3.991	4.444	3.772	3.518	3.459	3.781	3.617	3.621	2.825	2.825	2.873	3.040	3.736	3.874
Ca	-	-	-	-	0.097	-	-	-	-	-	-	-	-	-	-	-	-	-	-	-	-	-	-
Na	0.055	0 089	0.030	0.059	-	0.096	-	-	-	-	-	-	-	-	-	-	-	-	-	-	-	-	-
K	-	0.013	-	-	0.011	-	-	-	-	-	-	-	-	-	-	-	-	-	-	-	-	-	-
Sum (O)	6.065	6.097	6.039	6.084	5.713	5.946	5.414	5.419	5.619	5.667	5.898	6.059	5.933	5.930	6.059	6.017	6.024	5.998	6.009	5.912	5.907	6.035	6.036
Fe/SumR^{2+}	0.212	0.065	0.291	0.413	0.516	0.099	0.256	0.268	0.155	0.136	0.120	0.222	0.252	0.264	0.223	0.258	0.241	0.399	0.397	0.369	0.334	0.219	0.197

TABLE 3

Summary of experimentally determined chlorite compositional data as a function of oxygen and sulfur fugacity based on pyrrhotite compositions obtained from microprobe analyses. Mole fraction of daphnite calculated from data in table 2, as explained in the text. Abbreviations are the same as given for table 2

Run #	Temp (C)	Press (kb)	XDaph (+/- 1s)[1]	Buffer	Pyrrhotite NFeS (+/- 1s, n)	Log fS_2	Log fO_2
5B	600	2.07	0.256	PoMt	0.9410 (0.005, 15)	-3.42 (0.50)	-17.74 (0.38)
6B	600	2.07	0.268 (0.008)	PoMt	0.9430 (0.005, 8)	-3.61 (0.50)	-17.90 (0.38)
27A	600	2.07	0.155 (0.016)	PPM	0.9254 (0.002, 22)	-2.05 (0.20)	-16.44 (calc)
B	"	"	0.136 "	"	"	"	"
28A	600	2.07	0.120 (0.010)	PPM	0.9186 (0.005, 7)	-1.50 (0.50)	"
26(b)B	600	6.00	0.222 (0.004)	PPM	-	-	-16.41 (calc)
30A	600	6.00	0.252 (0.008)	PPM	0.9342 (0.007, 10)	-2.13 (0.60)	"
B	"	"	0.264 (0.014)	PPM	"	"	"
31A	600	6.00	0.223 (0.006)	PPM	0.9302 (0.005, 6)	-1.79 (0.43)	"
B	"	"	0.258 (0.016)	PPM	"	"	"
34B	600	6.00	0.241 (0.023)	PPM	-	-	"
36A	600	6.00	0.399 (0.044)	PoMt	0.9367 (0.005, 11)	-2.35 (0.44)	-17.05 (0.33)
B	"	"	0.397 (0.010)	PoMt	"	"	"
41A	575	4.50	0.369 (0.019)	PPM	0.9268 (calc)	-2.05 (calc)	-17.23 (calc)
B	"	"	0.334	PPM	"	"	"
42B	600	5.00	0.219 (0.006)	PPM	0.9279 (calc)	-1.76 (calc)	-16.48 (calc)
43B	625	5.50	0.197 (0.007)	PPM	0.9292 (calc)	-1.50 (calc)	-15.80 (calc)

[1] The standard deviation is based on an average of ten analyzed grains per run.

Sulfides.—Evidence for reaction in most runs is abundant and is deduced from optical examination of both sulfides and silicates. The most obvious sign of reaction is the breakdown of pyrite and disappearance of troilite in starting charges A and B.

Desulfidation of pyrite is indicated by pseudomorphous replacement of pyrite, sometimes complete, by pyrrhotite and overgrowths of pyrrhotite on magnetite indicating release of sulfur due to breakdown of pyrite. XRD analysis indicates that troilite has been sulfidized in all cases to a more sulfur-rich hexagonal pyrrhotite.

Pyrrhotite associated with chlorite forms rod-shaped grains (possibly plates of pyrrhotite observed from the side), which are distinctly different from the anhedral and granular pyrrhotite in the surrounding ground-

mass. Both pyrrhotites are compositionally identical. The abundance of pyrrhotite and magnetite in chlorite patches is excellent textural evidence that these iron minerals formed by oxidation and sulfidation of iron from the chlorite.

Most runs in table 1 equilibrated chlorite at the PPM fO_2–fS_2 buffer. Runs with a middle layer of PPM (3:3:2) always ended up with the PPM assemblage established in both ends of the inner capsule (charges A and B). Textures such as pyrrhotite–pyrite intergrowths and pyrrhotite replacing magnetite are common in these runs and demonstrate that the PPM buffer was stable at the elevated pressure and temperature condition for the long duration of many of the runs.

EXPERIMENTAL RESULTS

Chlorite.—Chlorite compositional data listed in table 2 were selected on the basis of measured shifts in the Fe/(Fe + Mg) ratios exceeding the sum of the standard deviations (table 3) in this ratio between initial and final chlorite compositions. These include 4 runs in which both $Fe/\Sigma R^{2+}$ and aluminum contents in charges A and B were reversed (27, 30, 36, and 41).

Initial and final chlorite compositions, based on 14 anhydrous oxygens, are plotted in figures 2, 3, and 4, adopted from Foster (1962). Foster's method is preferred to a simple comparison of Fe/(Fe + Mg) ratios, because it also demonstrates how the coupled substitutions in chlorite affect the distribution of Si and Al in the structure in response to changing $Fe/\Sigma R^{2+}$ ratios.

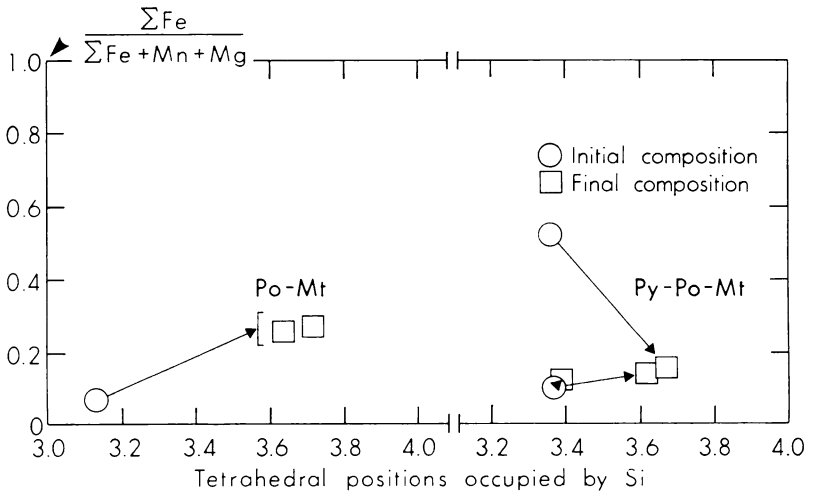

Fig. 2. Chlorite compositions from sulfidation and oxidation experiments buffered by pyrrhotite–magnetite (PoMt) and pyrite–pyrrhotite–magnetite (PPM) at 600°C and 2.07 kb. Chlorite compositions are expressed as the ratio of total iron:total divalent cations plotted against the number of tetrahedral positions occupied by silicon.

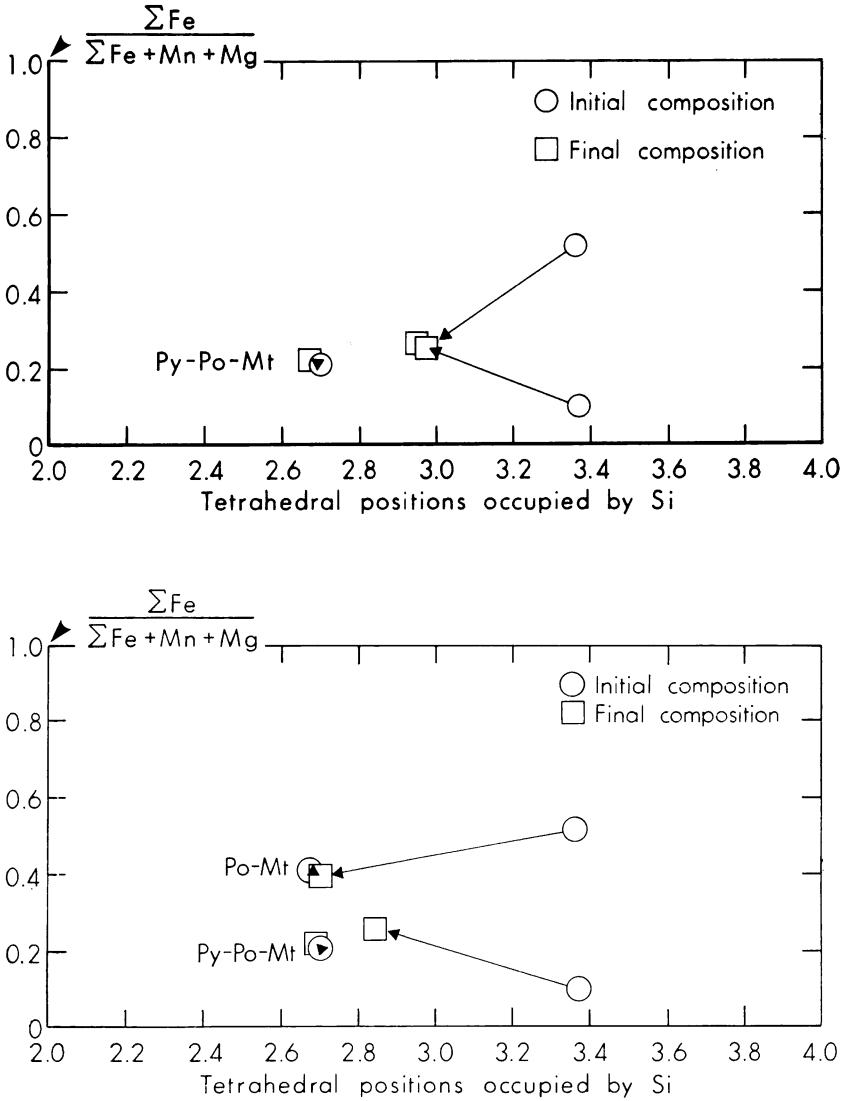

Fig. 3. Chlorite compositions from sulfidation and oxidation experiments buffered by PoMt and PPM at 600°C and 6.0 kb. Chlorite compositions expressed as in figure 2.

Figure 2 summarizes the results of sulfidation-oxidation experiments at 600°C and 2.07 kb. At the PPM invariant point, final $Fe/\Sigma R^{2+}$ ratios are remarkably consistent, suggesting that this ratio was indeed controlled by sulfidation-oxidation equilibria. Chlorite from runs 5B and 6B (fig. 2), for which the buffer was PoMt, have considerably higher $Fe/\Sigma R^{2+}$ ratios than were found in runs 27A, B and 28A which were buffered by PPM. From table 3 it can be seen that, in charges 5B and 6B, the sulfur and

oxygen fugacities were lower than those at the PPM invariant point, and chlorite in equilibrium with these lower fugacities should have a higher $Fe/\Sigma R^{2+}$ ratio.

Results of sulfidation-oxidation experiments at higher pressures and at three temperatures are given in figures 3 and 4. The $Fe/\Sigma R^{2+}$ ratio in chlorite has changed in response to sulfur and oxygen fugacities prevailing in the charges and clearly illustrates how very sensitive this ratio in chlorite is to the ambient conditions.

The Al and Si contents of the product chlorites are consistent with the mineral's structural formula. The chlorite structure consists of alternating talc-like sheets or 2:1 layers and brucite-like sheets or interlayers. The structure leads to the general formula $X_mY_4O_{10}(OH)_8$, with the talc-like sheets represented by $X_{\frac{m}{2}}Y_4O_{10}(OH)_2$ and the brucite-like sheets by $X_{\frac{m}{2}}(OH)_6$. X and Y represent octahedral and tetrahedral sites respectively (Deer, Howie, and Zussman, 1962). In these formulae m is usually 6 or less, but not more. Ideally, in order to maintain charge in the chlorite structure, an increase in Si should be accompanied by an equivalent decrease in tetrahedral Al, an equivalent increase in octahedral R^{3+}, generally Al^{3+}, and an equivalent decrease in octahedral R^{2+} in accordance with the following equation from Foster (1962):

$$[Si^{4+} + R^{2+} = R^{3+}(iv) + R^{3+}(vi)] .$$

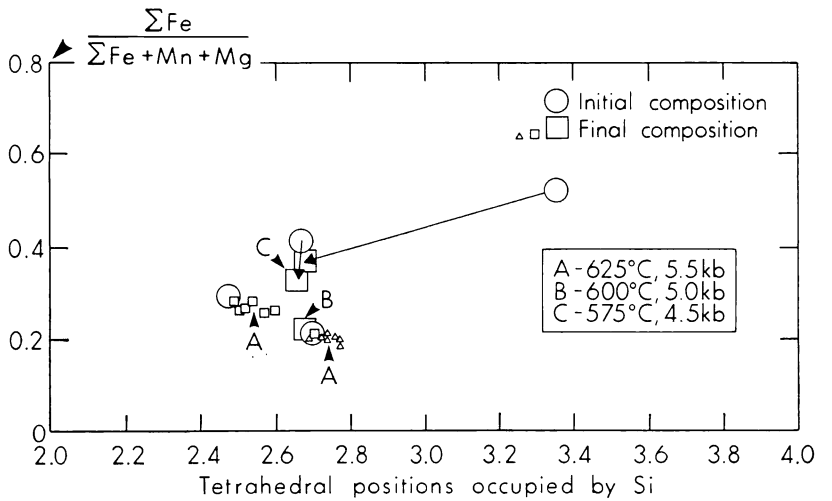

Fig. 4. Chlorite compositions from sulfidation and oxidation experiments buffered by PPM at 625°C, 5.5 kb (A); 600°C, 5.0 kb (B); and 575°C, 4.5 kb (C). Chlorite compositions are expressed as in figure 2. Small symbols are from experiment 43 at 625°C and 5.5 kb. Incomplete equilibration is indicated for the most aluminous chlorite starting composition in this experiment (43A, small squares), while the constant mole fraction of iron shown by the small triangles indicates equilibrium was reached for the starting chlorite composition in 43B.

The role of ferric iron in the chlorite structure has been discussed in detail by Foster (1962). Foster showed that in most cases where there was a deficiency of octahedral Al^{3+} relative to tetrahedral Al^{3+}, ferric iron proxies for the deficient Al^{3+} in a ratio of 1:1; that is, any ferric iron present in chlorite serves only to maintain charge balance in the chlorite structure and need not indicate oxidation of Fe^{2+} to Fe^{3+}.

Synthetic chlorites ranging in composition from Si:Al = 3:2 and Fe^{2+}:Mg = 0.20:0.80 were annealed by us at 600°C and 5 kb for 10 days, with the oxygen fugacity buffered by magnetite + hematite. Mossbauer spectroscopy revealed that the chlorite contained no appreciable ferric iron, less than 5 percent in the most iron-rich chlorite (R. G. Burns, personal commun., 1985). Therefore, our experimental results should be applicable to natural assemblages that formed at oxygen fugacities as high as those given by magnetite + hematite. At oxygen fugacities in excess of this buffer, such as occurs in certain hydrothermal regimes, a significant proportion of Fe^{2+} may be oxidized to Fe^{3+} (Walshe, 1986).

The effects of coupled substitutions in chlorite may be deduced from the compositions of Mg-rich chlorites produced in the 2.07 kb runs (fig. 2; table 3). These tend to be very silica rich as indicated by the number of tetrahedral positions occupied by Si and contain significantly less than the ideal complement of 6 cations in octahedral positions. In these runs, increase in the number of tetrahedral positions occupied by Si leads to a decrease in the negative charge on the tetrahedral sheets equivalent to [4.00–Si^{4+}(iv)]. Charge balance is maintained, however, by accommodating an excess of Al in the octahedral sheets. Consequently, Mg-rich chlorites from the 2.07 kb runs also contain a maximum number of tetrahedral positions occupied by Si and an excess of octahedral Al over tetrahedral Al. The deficiency in the ideal number of cations in octahedral positions is equivalent to one half the excess octahedral Al (analyses 5B and 6B in table 2).

The number of tetrahedral positions occupied by Si in chlorite from the 600°C, 6.0 kb experiments is considerably less than that from the 600°C, 2.07 kb experiments (compare figs. 2 and 3). The reasons for this are not obvious, but the previously described textural observations indicating that kyanite was partially consumed in the high pressure runs would seem to indicate that chlorite may be stabilized by incorporating more Al into tetrahedral sites relative to Si, as indicated by the decrease in the number of tetrahedral positions occupied by Si in figure 3. Caruso and Chernosky (1979) made a similar observation that the stability of serpentine is increased by substitution of Al for Si.

Sulfides.—Sulfides and chlorite came to equilibrium in the experiments as indicated by the consistency of their compositions in table 3. The apparently large analytical errors, up to 0.007 in N_{FeS} of pyrrhotite, are not unexpected in view of reported difficulties in quenching pyrrhotite compositions on and near the pyrrhotite–pyrite solvus (Scott, 1973). Log fS_2 values calculated for the pyrite–pyrrhotite equilibrium using the method of Froese and Gunter (1976) and from N_{FeS} data in table 3 are,

within limits of analytical error, virtually identical to those expected at the PPM invariant point (Bryndzia, ms).

Talc.—Almost without exception, all charges containing initial chlorite compositions more Mg-rich than Fe/(Fe + Mg) = 0.20 produced an assemblage of chlorite + talc +/− quartz +/− magnetite + pyrrhotite. The reaction of chlorite and quartz to produce talc is evident from the relative peak intensities of these phases in XRD traces of run products compared with starting compositions. Charges with Fe–chlorites in the same capsules and at the same fO_2–fS_2 conditions or with similar high Fe/(Fe + Mg) ratios at both ends of the same capsule produced an assemblage of chlorite + quartz + magnetite + pyrrhotite, that is, no talc. In charge 5B (Fe/(Fe + Mg) = 0.065), a chlorite + talc + spinel–magnetite(ss) assemblage resulted; no quartz remained at the end of the run suggesting that it was consumed by the talc forming reaction. The talc + chlorite + quartz assemblage present in charges 30B and 31B (table 1) is most likely metastable, resulting from incomplete consumption of quartz in the talc-forming reaction.

In summary, bulk compositions of charges A and B appear to be the controlling factors in determining phase mineralogy, including formation of talc. Regardless of bulk composition, however, the ambient fO_2–fS_2 conditions determine the Fe/(Fe + Mg) ratio in chlorite in the presence of aluminosilicate and quartz (table 3).

DISCUSSION AND APPLICATION OF RESULTS

Solution Model for Chlorite

The approach used in this paper to derive an activity expression for the daphnite component from a chlorite mineral analysis is adopted from Froese (1976) in which activity expressions are formulated in terms of a single iron atom in the pure iron endmember component.

Model 1.—In daphnite, iron and aluminum occupy five and one, respectively, of the six octahedral sites, namely: $[Fe_5Al][AlSi_3]O_{10}(OH)_8$, and are assumed to mix randomly over all six energetically equivalent octahedral sites. All the octahedral sites are assumed to be filled so that $\Sigma(Oct) = 6.00$. However, due to substitutions in chlorite such as R^{3+} for R^{2+} cations in octahedral sites, vacancies are possible so that $\Sigma(Oct)$ may be less than the ideal complement of 6.00 (Foster, 1962). Charge balance is maintained over the chlorite structure by coupled substitutions of R^{3+} cations, principally Al^{3+}, between octahedral and tetrahedral sites (Bailey, 1975). Aluminum in octahedral sites is the source of positive charge in the interlayer, which is balanced by aluminum in tetrahedral sites, the source of negative charge in the 2:1 layer. Therefore, by virtue of coupled substitutions in the chlorite structure dictated by structural and charge considerations, aluminum in octahedral sites is also related to silicon in tetrahedral sites, and mixing of silicon and aluminum in tetrahedral sites may be ignored (Holdaway, 1980). The proportion of the daphnite component in chlorite is therefore a function of the amount of iron and aluminum mixing randomly over six octahedral sites, not all of which

TABLE 4

Activities of the daphnite component in chlorite calculated using activity models discussed in the text and chlorite compositions given in table 2. The mole fraction of iron in chlorite is calculated as $Fe^{2+}/\Sigma R^{2+}$.

Run #	5B	6B	27A	27B	28A	26(b)B	30A	30B	31A
$Fe/\Sigma R^{2+}$	0.256	0.268	0.155	0.136	0.120	0.222	0.252	0.264	0.223
Model 1	0.216	0.229	0.143	0.126	0.117	0.224	0.247	0.259	0.225
Model 2	0.199	0.202	0.130	0.116	0.114	0.221	0.247	0.259	0.222

need to be filled due to R^{3+} cations substituting for R^{2+} cations. The expression derived for calculating the activity of daphnite (with a single iron atom in the formula), from a chlorite mineral analysis is therefore: $a_{Daph} = [Fe^{2+}/\Sigma(R^{2+} + R^{3+} + \square)/5/6)][Al(Oct)/\Sigma(R^{2+} + R^{3+} + \square)/1/6]^{1/5}$, where $\square$ indicates a vacant octahedral site.

Model 2.—This model is a variation of model 1. In addition to mixing of iron and aluminum on octahedral sites, this model also considers mixing of silicon and aluminum over four energetically equivalent tetrahedral sites, namely: a_{Daph} = [model 1][Si/3]$^{3/4}$[Al(T)]$^{1/4}$. Model 2 is essentially the same activity model adopted by Walshe (1986, table 5). Walshe's model, however, considers mixing of silicon and aluminum only over two of the four tetrahedral sites, with no mixing occurring on the remaining two tetrahedral sites which are always occupied by silicon (see also Walshe and Solomon, 1981).

The composition term against which model activities are conventionally compared is the mole fraction of a component in a given mineral. In the present case the component is daphnite, the iron endmember chlorite, and the mole fraction is represented by the $Fe/\Sigma R^{2+}$ ratio in chlorite. The analytical errors associated with this ratio are small, on the order of ± 0.01 to 0.03 (avg = 0.02). Model daphnite activities calculated for chlorite analyses in table 2 are summarized in table 4 and plotted in figure 5.

In figure 5, the heavy solid line has unit slope and represents the case of ideal ionic solution, that is, $a_{Daphnite} = X_{Daphnite}$. Data points for models 1 and 2 in figure 5 were subjected to linear regression analyses for which the lines of best fit were forced through the origin with the following results. Model 1: gradient (m) = 0.98, and correlation coefficient (r^2) = 0.994; Model 2: m = 0.962, and r^2 = 0.990.

The calculated model activities in figure 5 are in excellent agreement with the line of unit slope. The calculations are not very model sensitive. These models differ only in that model 2 considers mixing of silicon and aluminum in tetrahedral sites, whereas model 1 ignores mixing on tetrahedral sites. This strongly suggests that consideration of tetrahedral site mixing is not a very significant factor in determining the activity of the daphnite component, a point discussed in detail during the formulation of model 1. This is best illustrated by the fact that the activity of daphnite [$Fe_5Al_2Si_3O_{10}(OH)_8$] in pure thuringite [$Fe_4Al_4Si_2O_{10}(OH)_8$], which has the maximum Al-for-Si substitution, is 0.919 and 0.838 by models 1 and 2, respectively. It follows that only by substituting other R^{2+} ions for

TABLE 4 (continued)

31B	34B	36A	36B	41A	41B	42B	43B	Daphnite	Thuringite
0.258	0.241	0.399	0.397	0.369	0.334	0.219	0.197	1.000	1.000
0.259	0.241	0.396	0.395	0.357	0.324	0.219	0.197	1.000	0.919
0.258	0.238	0.391	0.391	0.352	0.319	0.216	0.195	1.000	0.828

Fe^{2+} can the activity of daphnite be appreciably changed using these models and explains much of the excellent correlation observed in figure 5.

In the absence of an independent (thermodynamic) measure for the activity of the daphnite component, it is not possible to say whether solution of the daphnite component in chlorite is truly ideal, or whether models 1 and 2 correlate very well (fig. 5), simply because the $Fe/\Sigma R^{2+}$ factor is dominant in both models. More data of this same type will not resolve the problem because these chlorites cover a large range of variation in both tetrahedral and octahedral site occupancies. Chlorite com-

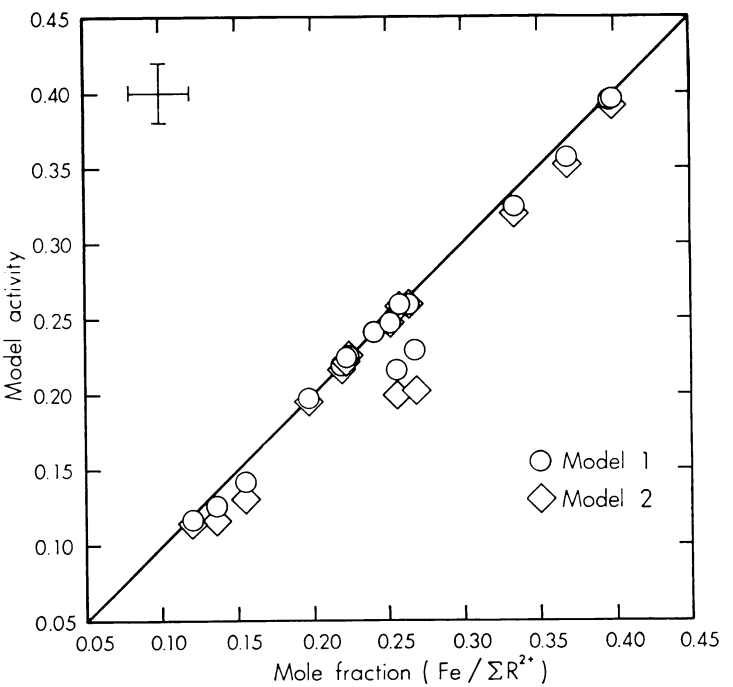

Fig. 5. Plot of the mole fraction of iron in chlorite versus activities of the daphnite component from models 1 and 2. The solid line has unit slope and represents ideal solid solution. The minimum estimated error in both the mole fraction of iron in chlorite and calculated model activities is ± 0.02 and is indicated by the error bars. Points are calculated model activities (see text). Model 1 gives a result that is indistinguishable from ideality.

positions from the literature (Deer, Howie, and Zussman, 1962) show the same good correlation as those in figure 5.

In order to test the ideal ionic solution hypothesis further, values of equilibrium constants for the oxidation reaction (eq 2, below) were calculated from experimental data at 600°C and 6.0 kb given in table 3. For eight chlorites ranging in composition from Fe/(Fe + Mg) = 0.222 to 0.399, $\log K_{(2)}$ is 5.84 ± 0.06 (± 1s, n = 8); that is, within the limits of experimental error, the data yield a constant value for $\log K_{(2)}$, a result that is consistent with, but does not prove, the ideal ionic solution hypothesis.

In the absence of independent activity determinations, however, it is reasonable to conclude that chlorites can be satisfactorily represented by an ideal mixing model such as model 1, which gives an activity indistinguishable from the mole fraction of iron in chlorite. In spite of the fact that the mole fraction of iron in chlorites predicts unit activity for any pure iron chlorite (which cannot be true), deviations from the mole fraction of iron caused by Al/Si variations are apparently negligible as suggested by the constant value obtained for $\log K_{(2)}$.

THERMOCHEMISTRY

The two reactions that describe chlorite compositions as a function of fO_2 and fS_2 written in terms of sulfidation and oxidation of the Fe-endmember chlorite component, daphnite, are:
Sulfidation (in the pyrrhotite field):

$$FeAl_{2/5}Si_{3/5}O_2(OH)_{8/5}\ (\text{in Fe–Mg chlorite}) + 1/2S_2 = FeS\ (\text{in pyrrhotite}) + 1/5Al_2SiO_5 + 2/5SiO_2 + 4/5H_2O + 1/2O_2 \quad (1)$$

Sulfidation under conditions of higher fS_2 (in the pyrite field):

$$FeAl_{2/5}Si_{3/5}O_2(OH)_{8/5}\ (\text{in Fe–Mg chlorite}) + S_2 = FeS_2 + 1/5Al_2SiO_5 + 2/5SiO_2 + 4/5H_2O + 1/2O_2 \quad (1')$$

Oxidation (in the magnetite field):

$$FeAl_{2/5}Si_{3/5}O_2(OH)_{8/5}\ (\text{in Fe–Mg chlorite}) + 1/6O_2 = 1/3Fe_3O_4 + 1/5Al_2SiO_5 + 2/5SiO_2 + 4/5H_2O \quad (2)$$

Combining reactions (1) and (2) yields the equilibrium relation between magnetite and pyrrhotite:

$$Fe_3O_4 + 3/2S_2 = 3FeS + 2O_2 \quad (3)$$

In reactions (1), (1′), and (2), the daphnite component in chlorite reacts with either sulfur or oxygen to form a chlorite enriched in Mg. Concurrently, reaction (3) is a "sliding-scale" buffer for which the non-stoichiometric composition of pyrrhotite can be used to define the fS_2 and also fO_2 if pure magnetite is present. Under conditions of higher fS_2 a fourth reaction will take place:

$$FeS + 1/2S_2 = FeS_2\,. \quad (4)$$

Coexisting pyrite, pyrrhotite, and magnetite define an invariant three-phase assemblage in the Fe–S–O system at a given pressure and temperature, where the fS_2, fO_2, and activity of FeS are all defined at equilibrium.

The important variables fO_2 and fS_2 may be calculated for reactions (1), (1′), and (2) for any activity of daphnite at any pressure and temperature, as follows:

For reaction (1)

$$\log K_{(1)} = 1/2\log fO_2 + 4/5\log fH_2O + \log a_{FeS} - 1/2\log fS_2 - \log a_{Daphnite} \quad (5)$$

and

$$\log fO_2 = \log fS_2 + 2\log K_{(1)} + 2\log a_{Daphnite} - 8/5\log fH_2O - 2\log a_{FeS}\,. \quad (6)$$

For reaction (1′)

$$\log K_{(1')} = 1/2\log fO_2 + 4/5\log fH_2O - \log fS_2 - \log a_{Daphnite} \quad (5')$$

and

$$\log fO_2 = 2\log fS_2 + 2\log K_{(1')} - 8/5\log fH_2O + 2\log a_{Daphnite}\,. \quad (6')$$

For reaction (2)

$$\log K_{(2)} = 4/5\log fH_2O - 1/6\log fO_2 - \log a_{Daphnite} \quad (7)$$

and

$$\log fO_2 = 24/5\log fH_2O - 6\log K_{(2)} - 6\log a_{Daphnite}\,. \quad (8)$$

The effect of confining pressure on reactions (1), (1′), and (2) is calculated from the relation

$$\log K_{P_2} - \log K_{P_1} = -\Delta V_s^\circ \times (P_2\text{-}P_1)/2.303RT \quad (9)$$

where $P_1 = 1$ bar and ΔV_s° is the standard molar volume change of solid phases in the reaction at 298.15K and 1 bar.

Enthalpy, Free Energy, and Absolute Entropy of Formation of Daphnite, at 298.15 and 1 Bar

Values of $\log K_{(2)}$ were calculated at 1 bar and 625°, 600°, and 575°C from solution of eqs (7) and (9). The standard state for the solids is pure endmember composition at temperature and 1 bar, and mixing of the species in the vapor phase is ideal (that is, $\Delta H_{mix}^\circ = 0$).

Activities of daphnite were calculated assuming ideal ionic solution of the daphnite component in chlorite; the fugacity of water is from Burnham, Holloway, and Davis (1969); the oxygen fugacities were calculated at P and T for the PPM invariant point and PoMt equilibrium, following the method of Froese (1976), and are given in table 3; the molar volume data for all phases except daphnite is from Robie, Hemingway, and Fisher (1979) whereas the molar volume for daphnite is from McOnie, Fawcett, and James (1975). Results are plotted against 1/T(K) in figure 6.

The regression equation for the line of best fit in figure 6 is given by:

$$\log K_{(2)} = 8.101 - 1.974 \times 10^3/T \quad (10)$$

and is assumed to be linear down to 298.15 K.

The standard state enthalpy of reaction ($\Delta H_r°$) is defined by the expression:

$$d\log K_{(2)}/d(1/T) = -\Delta H_r°/2.303R \quad (11)$$

where R is the gas constant.

The value of $\Delta H_r°$ for the oxidation reaction (2) was used to calculate the enthalpy of formation for daphnite [$Fe_5Al_2Si_3O_{10}(OH)_8$] from the elements at 298.15 K and 1 bar. Enthalpy data for product phases at 298.15 K and 1 bar are from Robie, Hemingway, and Fisher (1979). The calculated enthalpy of formation for daphnite is −1726.3 kcal/mole. As a consequence of the limited temperature interval over which the oxidation reaction was studied (50°C), it is difficult to estimate meaningful errors for the calculated enthalpy, particularly since most of the data used in constructing figure 6 are from experiments at a single temperature of 600°C. If it is assumed that errors of comparable magnitude pertain to the other data points in figure 6 as for 600°C (873.15 K), then a reasonable error estimate for the calculated enthalpy value is ± 11 kcal/mole.

Values of $\Delta G_r°$ were calculated from logK's used in figure 6 and are plotted against T(K) in figure 7. The regression equation for the line of best fit to the data in figure 7 is given by:

$$\Delta G_r° \text{ (kcal)} = 9.103 - 0.037T. \quad (12)$$

The free energy of formation ($\Delta G_f°$) of daphnite was calculated from the free energy of reaction of eq (2) obtained by solution of eq (12) for the three temperatures given in figure 7. With the free energy of formation of product phases from Robie, Hemingway, and Fisher (1979) and solution

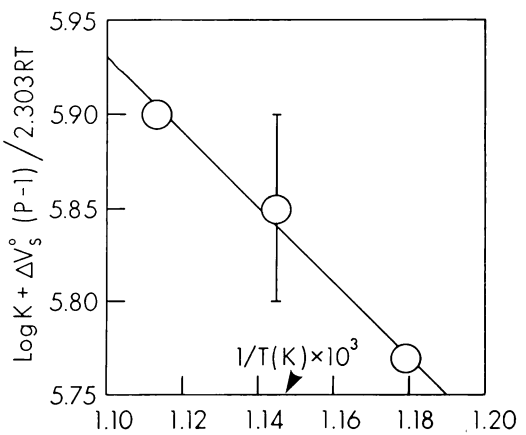

Fig. 6. Log $K_{(2)}$ versus $10^3/T(K)$ plot derived from solution of eqs (7) and (9) at 625°, 600°, and 575°C, with activities of the daphnite component calculated assuming ideal ionic solution of the daphnite component in chlorite. Error estimate represents the range in log $K_{(2)}$ at 600°C. See text for explanation.

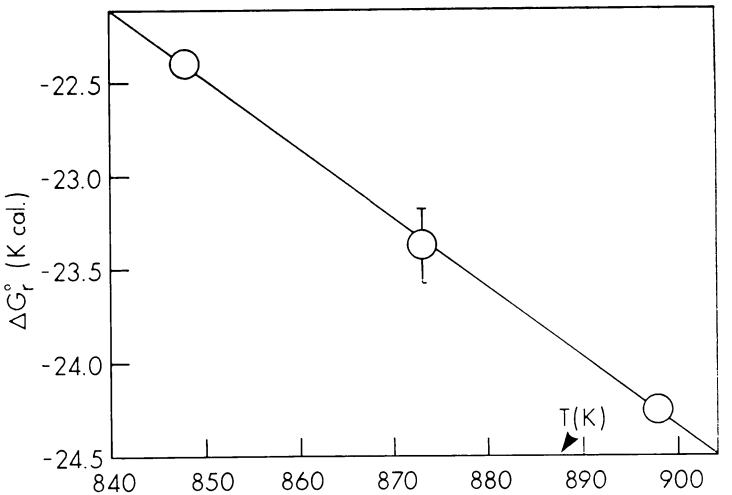

Fig. 7. ΔG°_r versus T(K) plot calculated from the data in figure 6. See text for explanation.

of the relationship $\Delta G_r^\circ = \Sigma\Delta G_f^\circ$(products) $-\Sigma\Delta G_f^\circ$(reactants), the following regression equation for the free energy of formation of daphnite is obtained:

$$\Delta G_f^\circ{}_{(\text{Daphnite, 1 bar})} \text{ (kcal/mole)} = -1767.7 + 0.560T \qquad (13)$$

By extrapolation of eq (13), the standard state free energy of formation of daphnite, from the elements at 298.15 K and 1 bar, is -1600.7 ± 6.4 kcal/mole.

From the relationship $(\Delta G_f^\circ - \Delta H_f^\circ)/T = -\Delta S_f^\circ$, obtained by substituting values of ΔG_f° and ΔH_f° calculated previously at 298.15 K and 1 bar, together with standard entropies of the elements from Robie, Hemingway, and Fisher (1979), the absolute standard state entropy of formation of daphnite (S_f°) at 298.15 K and 1 bar is calculated to be 142.2 ± 13 cal/mol/K.

Geological Application to Metamorphosed Sulfide Ores, Ducktown, Tenn.

Our results can be applied directly to geological problems by solving eqs (6), (6′), and (8) for a_{Daph}, for chlorite which contains no appreciable ferric iron and coexists with quartz, aluminosilicate, and opaque phases such as Fe-oxide, Fe-Ti oxide, and/or an Fe-sulfide. Because the ratio $Fe^{2+}/\Sigma R^{2+}$ in chlorite is so sensitive to fO_2 and fS_2, the results of such a calculation are best represented as isopleths of X_{Daph} (mole fraction of the daphnite component) on an isobaric-isothermal $\log fO_2$-$\log fS_2$ diagram, such as figure 8 for example. Our choice of figure 8 will become apparent in the following discussion. Several features of figure 8 are noteworthy.

The commonly observed trend of decreasing Fe/(Fe + Mg) in chlorite approaching an ore body is consistent with increasing oxygen fugacity in the magnetite field, increasing oxygen and sulfur fugacity for coexisting

magnetite and pyrrhotite, or increasing sulfur fugacity in the pyrrhotite field, at a given pressure and temperature. The topology of chlorite isopleths on figure 8 is such that, in the magnetite field, relatively large variations in fO_2 produce only minor changes in X_{Daph} in chlorite, as opposed to the dramatic variations in X_{Daph} caused by very small changes in fS_2 in the pyrrhotite field. A unique chlorite composition is defined by the fO_2–fS_2 invariant assemblage of coexisting pyrite, pyrrhotite, and magnetite (PPM) at a given pressure and temperature. Bryndzia and Scott (1986) have shown that the X_{Daph} in a chlorite–PPM assemblage is a sensitive function of temperature and a useful geothermometer.

We have chosen to apply our experimental chlorite data to the metamorphosed massive sulfide ore bodies of Ducktown, Tenn. The regional geology, metamorphic petrology, mineral chemistry, and volatile phase equilibria of the ores and country rocks have been documented and discussed elsewhere by Nesbitt and Kelly (1980), Nesbitt (1982), and Nesbitt and Essene (1983). Only data pertaining to the chlorite-bearing assemblages are considered here. The conditions of metamorphism for the Ducktown ores and country rocks are: $T = 550 \pm 40°C$, $P_{Total} = P_{fluid} = 6.0 \pm 1$ kb; $X_{H_2O} = 0.84$ (Nesbitt and Essene, 1983; table 4). The fluid was

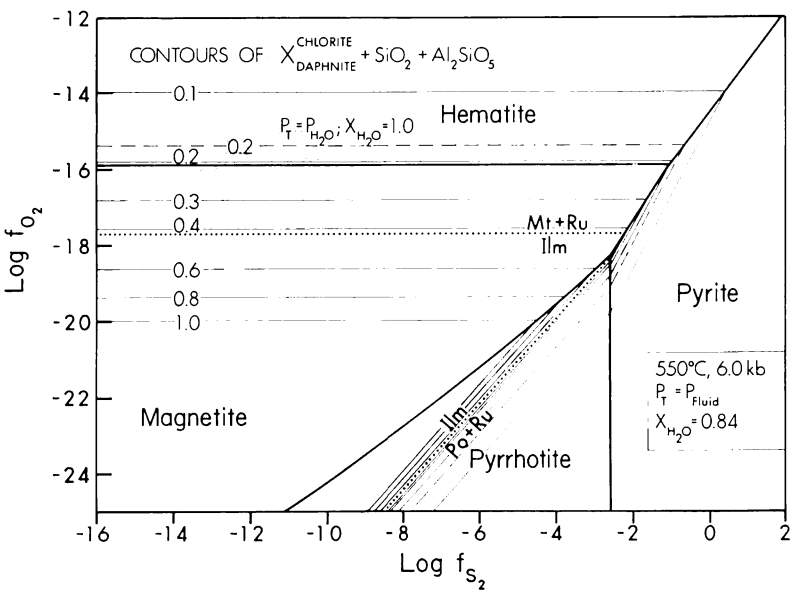

Fig. 8. Calculated stability of chlorite plotted as isopleths of the daphnite component in chlorite ($X_{Daph} = Fe/\Sigma R^{2+}$) in the Fe–Ti–O–S system at 550°C, $P_{Total} = P_{fluid} = 6.0$ kb; $X_{H_2O} = 0.84$. Method of calculation adopted from Froese (1977). Standard state free energies and molar volumes for magnetite, ilmenite, rutile, and hematite are from Robie, Hemingway, and Fisher (1979). The standard Gibbs free energy changes for the pyrrhotite–vapor and pyrite–pyrrhotite equilibrium are from Froese and Gunter (1976). The standard state free energy of formation of daphnite is from this study as explained in the text. Molar volume of daphnite is from McOnie, Fawcett, and James (1975). Fugacities are in bars. The dashed line is the 0.2 chlorite isopleth calculated for $X_{H_2O} = 1.0$.

diluted by CO_2 due to oxidation of graphite in the country rocks during regional metamorphism. As a consequence of regional metamorphism and variations in fO_2 and fS_2 in the ore and wall rocks, Fe-Ti oxides, Fe-sulfides, and ferromagnesian silicate compositions ($Fe/\Sigma R^{2+}$) are zoned about the ores. Chlorite in the wall rocks is characterized by the assemblage pyrrhotite–ilmenite and $Fe/\Sigma R^{2+}$ in chlorite ranges from 0.51 to 0.40, avg 0.46. Closer to the ore, ilmenite is replaced by rutile according to the following reaction:

$$\text{ilmenite} + 1/2S_2 = \text{pyrrhotite} + \text{rutile} + 1/2O_2 \qquad (14)$$

and $Fe/\Sigma R^{2+}$ in chlorite ranges from 0.40 to 0.22, avg 0.32. Locally around the ores a third characteristic assemblage is observed, consisting of pyrite–pyrrhotite–rutile and $Fe/\Sigma R^{2+}$ in chlorite ranges from 0.28 to 0.14, avg 0.22. The transition of ilmenite to rutile (in the pyrrhotite field) described by eq (14) must therefore occur in rocks in which $Fe/\Sigma R^{2+}$ of chlorite is close to 0.40 (Nesbitt, 1982; table 1). Agreement between the chlorite composition at this transition predicted by our calculations in figure 8 ($Fe/\Sigma R^{2+} = 0.42$) and that reported by Nesbitt based on field observation ($Fe/\Sigma R^{2+} = 0.40$) is remarkably good.

In addition to the very sensitive nature of $Fe/\Sigma R^{2+}$ in chlorite to fO_2 and fS_2, the composition of the fluid phase must also be considered. As an example, in figure 8 the $Fe/\Sigma R^{2+} = 0.2$ isopleth calculated for $P_{Total} = P_{Fluid}$ and $X_{H_2O} = 1.0$ plots approx 0.4 log units higher in fO_2 (in the magnetite field) relative to the 0.2 isopleth calculated for $X_{H_2O} = 0.84$. The effect of diluting a fluid assumed to be pure water is to lower chlorite stability in $\log fO_2$-$\log fS_2$ space. A slightly lower value of X_{H_2O} than that determined by Nesbitt and Essene (1983) would result in the convergence of the predicted chlorite composition in figure 8 with that observed in the wall rocks. Within the limits of uncertainty (primarily in temperature), however, phase relations in figure 8 suggest that equilibrium was obtained for the chlorite–sulfide–oxide assemblage in the wall rocks of the Ducktown sulfide ores. Phase relations in figure 8 are also compatible with data from Mohr and Newton (1983) for sulfidic schists of the Anakeesta Formation, where $Fe/\Sigma R^{2+}$ of chlorite of 0.42 to 0.35 is in equilibrium with rutile + ilmenite + graphite + pyrrhotite in a staurolite-kyanite zone of metamorphism similar to that at Ducktown.

In summary, our experiments have shown that bulk composition is the controlling factor in determining phase mineralogy and that the $Fe^{2+}/\Sigma R^{2+}$ ratio in chlorite is sensitive only to fO_2 and fS_2. Our results are in complete agreement with Nesbitt's (1982) observation that chlorite at Ducktown is a primary metamorphic mineral which has preserved its peak metamorphic composition and is not the product of retrograde re-equilibration, even though coexisting pyrrhotite has certainly re-equilibrated. The utility of chlorite as a reliable indicator of fO_2 and fS_2 attending metamorphism of massive sulfide ores and adjacent wall rocks at Ducktown has been demonstrated. Successful application of our experimental results is contingent upon recognizing compositional variations in

chlorite ($Fe/\Sigma R^{2+}$) related to specific assemblages of Fe oxides/sulfides and Fe-Ti oxides and to the presence of graphite or carbonate which may indicate a fluid phase in which the mole fraction of water was less than unity.

ACKNOWLEDGMENTS

We are grateful to the following individuals for their advice during the course of this research and their numerous comments on previous drafts of this manuscript: G. M. Anderson, E. Froese, J. J. Fawcett, J. C. Rucklidge, A. J. Naldrett, and P.-Y. F. Robin. Discussions with J. M. Allen, J. K. Böhlke, M. S. Cho, B. Nesbitt, I. Hutcheon, R. S. James, G. B. Skippen, P. G. Spry, J. Walshe, and F. J. Wicks were also most helpful. Mineral specimens were kindly provided by F. J. Wicks and T. Ottaway (Royal Ontario Museum), D. H. Gorman (University of Toronto) and G. E. Harlow (American Museum of Natural History). We thank Subhash Shanbhag and Brian O'Donovan for drafting and photography. Financial support to Bryndzia was provided primarily by the University of Toronto through Open Doctoral Fellowships and an H. G. Ellsworth Fellowship in Mineralogy. This research was funded by NSERC Operating Grant no. A7069 awarded to Scott. Clarity of presentation and reasoning benefitted considerably from reviews by J. V. Chernosky, D. W. Mohr, and R. K. Popp.

REFERENCES

Allen, J. M., and Fawcett, J. J., 1982, Zoisite–anorthite–calcite stability relations in H_2O–CO_2 fluids at 5000 bars: an experimental and SEM study: Jour. Petrology, v. 23, p. 215-239.

Annersten, H., 1968, A mineral chemical study of a metamorphosed iron formation in northern Sweden: Lithos, v. 1, p. 374-397.

Bachinski, D. J., 1976, Metamorphism of cupriferous iron sulfide deposits, Notre Dame Bay, Newfoundland: Econ. Geology, v. 71, p. 443-452.

Bailey, S. W., 1975, Cation ordering and pseudo-symmetry in layer silicates: Am. Mineralogist, v. 60, p. 175-187.

Bird, G. W., ms, 1971, Metamorphic reactions in the system K_2O–MgO–Al_2O_3–SiO_2–H_2O at water pressures to 10 kb: Ph.D. thesis, Univ. Toronto, 121 p.

Bryndzia, L. T., ms, 1985, The composition of chlorite as a function of sulfur and oxygen fugacity: an experimental study with application to metamorphosed sulfide ores, Snow Lake area, Manitoba: Ph.D. thesis, Univ. Toronto, 124 p.

Bryndzia, L. T., and Scott, S. D., 1987, Application of chlorite–sulfide–oxide equilibria to metamorphosed sulfide ores, Snow Lake area, Manitoba: Econ. Geology, v. 82, in press.

Burnham, C. W., Holloway, J. R., and Davies, N. F., 1969, Thermodynamic properties of water to 1000°C and 10,000 bars: Geol. Soc. America Spec. Paper, v. 132, 96 p.

Caruso, L. J., and Chernosky, J. V., Jr., 1979, The stability of Lizardite: Canadian Mineralogist, v. 17, p. 757-769.

Chinner, G. A., 1960, Pelitic gneisses with varying ferrous/ferric ratios from Glen Clova, Angus, Scotland: Jour. Petrology, v. 1, p. 178-217.

Clark, T., and Naldrett, A. J., 1972, The distribution of Fe and Ni between synthetic olivine and sulfide at 900°C: Econ. Geology, v. 67, p. 939-952.

Craig, J. R., and Gilbert, M. C., 1974, Amphiboles in Appalachian ores [abs.]: Geol. Soc. America Abs. with Programs, v. 6, p. 346.

Deer, W. A., Howie, R. A., and Zussman, J., 1962, Rock-forming Minerals, v. 3, Sheet Silicates: London, Longman Group Ltd., 270 p.

Fawcett, J. J., Davies, I., and James, R. S., 1971, A modified closure for high-pressure cold-seal pressure vessels: Mineralog. Mag., v. 38, p. 529-531.

Fleming, P. D., and Fawcett, J. J., 1976, Upper stability of chlorite + quartz in the system MgO–FeO–Al_2O_3–SiO_2–H_2O at 2 kbars water pressure: Am. Mineralogist, v. 61, p. 1175-1193.

Foster, M. D., 1962, Interpretation of the composition and a classification for the chlorites: U.S. Geol. Survey Prof. Paper 414A, 33 p.

Froese, E., 1971, The graphical representation of sulfide–silicate phase equilibria: Econ. Geology, v. 66, p. 335-341.

———— 1976, Applications of thermodynamics in metamorphic petrology: Canada Geol. Survey Paper 75-43, 37 p.

———— 1977, Oxidation and sulfidation reactions, *in* Greenwood, H. J., ed., Application of thermodynamics to petrology and ore deposits: Mineralog. Assoc. of Canada Short Course Handbook, v. 2, p. 84-98.

Froese, E., and Gunter, A. E., 1976, A note on the pyrrhotite–sulfur vapor equilibrium: Econ. Geology, v. 71, p. 1589-1594.

Guidotti, C. V., 1974, Transition from staurolite to sillimanite zone, Rangeley Quadrangle, Maine: Geol. Soc. America Bull., v. 85, p. 474-490.

Hammarback, S., and Lindqvist, B., 1972, The hydrothermal stability of annite in the presence of sulfur: Geol. Foren. Forh., v. 94, p. 549-564.

Holdaway, M. J., 1980, Chemical formulae and activity models for biotite, muscovite and chlorite applicable to pelitic rocks: Am. Mineralogist, v. 65, p. 711-719.

Hounslow, A. W., and Moore, J. M., 1967, Chemical petrology of Grenville schists near Fernleigh, Ontario: Jour. Petrology, v. 8, p. 1-28.

Hutcheon, I., 1979, Sulfide–oxide–silicate equilibria; Snow Lake, Manitoba: Am. Jour. Sci., v. 279, p. 643-665.

Hutchison, M. N., ms, 1978, Refinement and application of the sphalerite geobarometer: Ph.D. thesis, Univ. Toronto, 159 p.

Kalogeropoulos, S. I., ms, 1982, Chemical sediments in the hanging wall of volcanogenic massive sulfide deposits: Ph.D. thesis, Univ. of Toronto, 488 p.

Kanehira, K. S., Banno, S., and Nishida, K., 1964, Sulfide and oxide minerals in some metamorphic terranes in Japan: Japanese Jour. Geology, v. 68, p. 1075-1088.

Koo, J., and Mossman, D., 1975, Origin and metamorphism of the Flin Flon stratabound Cu–Zn sulfide deposis, Saskatchewan and Manitoba: Econ. Geology, v. 70, p. 48-62.

Kramm, U., 1973, Chloritoid stability in manganese rich low-grade metamorphic rocks, Venn-Stavelot Massif, Ardennes: Contr. Mineralogy Petrology, v. 41, p. 179-196.

Kullerud, G., 1971, Experimental techniques in dry sulfide research, *in* Ulmer, G., ed., Research Techniques for High Pressure and High Temperature: New York, Springer-Verlag, p. 288-315.

Kullerud, G., and Yoder, H. S., 1963, Sulfide–silicate relations: Carnegie Inst. Washington Year Book 62, p. 215-218.

———— 1964, Sulfide–silicate relations: Carnegie Inst. Washington Year Book 63, p. 218-222.

Large, R. R., 1975, Zonation of hydrothermal minerals at the Juno Mine, Tennant Creek Goldfield, Central Australia: Econ. Geology, v. 70, p. 1387-1413.

Luth, W. C., and Tuttle, O. F., 1963, Externally heated cold-seal pressure vessels for use up to 10,000 bars and 750°C: Am. Mineralogist, v. 204, p. 8-13.

McDonald, J., 1967, Metamorphism and its effects on sulfide assemblages: Mineralium Deposita, v. 2, p. 200-220.

Mallio, W. J., and Gheith, M. A., 1972, Textural and chemical evidence bearing on sulfide–silicate reactions in metasediments: Mineralium Deposita, v. 7, p. 13-17.

Marmo, V., 1957, Geology of the Nokia region, south-west Finland: Comm. Geol. Finlande Bull., v. 176, p. 1-38.

———— 1960, On the sulfide-graphite schists of Finland: Comm. Geol. Finlande Bull., v. 190, p. 1-180.

McOnie, A. W., Fawcett, J. J., and James, R. S., 1975, The stability of intermediate chlorite of the clinochlore–daphnite series at 2 kb PH_2O: Am Mineralogist, v. 60, p. 1047-1063.

Mohr, D. W., and Newton, R. C., 1983, Kyanite–staurolite metamorphism in sulfidic schists of the Anakeesta Formation, Great Smokey Mountains, North Carolina: Am. Jour. Sci., v. 283, p. 97-134.

Mueller, R. F., 1960, Compositional characteristics and equilibrium relations in mineral assemblages of a metamorphosed iron formation: Am. Jour. Sci., v. 258, p. 449-497.

Naldrett, A. J., and Brown, G. M., 1968, Reaction between pyrrhotite and enstatite–ferrosilite solid solutions: Carnegie Inst. Washington Year Book 66, p. 427-429.

Nash, J. T., 1973, Microprobe analyses of sericite, chlorite and epidote from Jerome, Arizona: U.S. Geol. Survey Jour. Research, v. 1, p. 673-678.

Nesbitt, B. E., 1982, Metamorphic sulfide–silicate equilibria in the massive sulfide deposits at Ducktown, Tennessee: Econ. Geology, v. 77, p. 364-378.

Nesbitt, B. E., and Essene, E. J., 1983, Metamorphic volatile equilibria in a portion of the Southern Blue Ridge Province: Am. Jour. Sci., v. 283, p. 135-165.

Nesbitt, B. E., and Kelly, W. C., 1980, Metamorphic zonation of sulfides, oxides and graphite in and around the orebodies of Ducktown, Tennessee: Econ. Geology, v. 75, p. 1010-1021.

Peltola, E., 1960, On the black schists in the Outokumpu region in eastern Finland: Comm. Geol. Finlande Bull., v. 192, p. 1-107.

Popp, R. K., 1976, Wall-rock alteration associated with massive sulfide deposits, Ducktown, Tennessee: Carnegie Inst. Washington Year Book 76-77, p. 603-607.

Popp, R. K., and Gilbert, M. C., 1974, Sulfurization of intermediate Fe–Mg amphiboles [abs.]: Geol. Soc. America Abs. with Programs, v. 6, p. 1058.

Popp, R. K., Gilbert, M. C., and Craig, J. R., 1977, Stability of Fe–Mg amphiboles with respect to sulfur fugacity: Am. Mineralogist, v. 62, p. 13-30.

Rajamani, V., 1976, Distribution of Fe, Co and Ni between synthetic sulfide and orthopyroxene at 900°C: Econ. Geology, v. 71, p. 795-802.

Robie, R. A., Hemingway, B. S., and Fisher, J. R., 1979, Thermodynamic properties of minerals and related substances at 298.15 K and 1 bar (10^5 pascals) pressure and at higher temperatures: U.S. Geol. Survey Bull., v. 1452, 455 p.

Rumble, D., 1974, Gradients in the chemical potentials of volatile components between sedimentary beds of the Clough Formation, Black Mountain, New Hampshire: Carnegie Inst. Washington Year Book 73, p. 371-380.

———— 1976, Oxide minerals in metamorphic rocks, *in* Rumble, D., III., ed., Oxide Minerals: Mineralog. Soc. America Short Course Notes, v. 3, p. R1-R24.

Scott, S. D., 1973, Experimental calibration of the sphalerite geobarometer: Econ. Geology, v. 68, p. 466-474.

———— 1974, Experimental methods in sullfide synthesis, *in* Ribbe, P. H., ed., Sulfide Mineralogy: Mineralog. Soc. America Short Course Notes, v. 1, p. S1-S38.

———— 1975, Hydrothermal synthesis of refractory sulfide minerals: Fortschr. Mineral., v. 52, Spec. Issue, Internat. Mineral. Assoc. Gen. Mtg., 9th, Berlin-Regensberg 1974, Papers and Proc., p. 185-195.

Smith, D. G. W., 1969, Pyrometamorphism of phyllites by a dolerite plug: Jour. Petrology, v. 10, p. 20-53.

Spry, P. G., and Scott, S. D., 1986, The stability of zincian spinels in sulfide systems and their potential as exploration guides for metamorphosed massive sulfide deposits: Econ. Geology, v. 81, p. 1446-1463.

Statham, P. J., ms, 1975, Quantitative x-ray energy spectrometry: the application of Si(Li) detector to electron microprobe analysis: Ph.D. thesis, Univ. Cambridge, 225 p.

Thompson, J. B., Jr., 1972, Oxides and sulfides in regional metamorphism of pelitic schists: Internat. Geol. Cong., 24th, Montreal, 1972, sec. 10, p. 27-35.

Toulmin, P., III, and Barton, P. B., Jr., A thermodynamic study of pyrite and pyrrhotite: Geochim. et Cosmochim. Acta, v. 28, p. 641-671.

Tso, J. L., Gilbert, M. C., and Craig, J. R., 1979, Sulfidation of synthetic biotites: Am. Mineralogist, v. 64, p. 304-316.

Tuttle, O. F., 1949, Two pressure vessels for silicate-water studies: Geol. Soc. America Bull., v. 60, p. 1727-1729.

Walshe, J. L., 1986, A six-component chlorite solid solution model and the conditions of chlorite formation in hydrothermal and geothermal systems: Econ. Geology, v. 81, p. 681-703.

Walshe, J. L., and Solomon, M., 1981, An investigation into the environment of formation of the volcanic-hosted Mt. Lyell copper deposits, using geology, mineralogy, stable isotopes, and a six-component chlorite solid-solution model: Econ. Geology, v. 76, p. 246-284.